

# Numerical modelling of acoustic and ultrasound scattering problems with an arbitrarily shaped scatterer

**Abstract.** The application of the standard boundary element method to analyse in 2D space the acoustic high-frequency scattering problems by a rigid convex and concave scatterer illuminated by the plane wave is considered in this paper. The analysis is presented on the example of a flat wave illuminating an object under different angles. The solution for different wavenumbers and different scatterers was analysed and illustrated. The usefulness of such a simulation method was discussed from the acoustical tomography point of view.

**Streszczenie.** W artykule rozważono zastosowanie standardowej metody elementów brzegowych do analizy w przestrzeni 2D problemów rozpraszania akustycznego wysokich częstotliwości przez sztywny wypukły i wklęsły rozpraszacz oświetlony falą płaską. Analiza została przedstawiona na przykładzie fali płaskiej oświetlającej obiekt pod różnymi kątami. Przeanalizowano i zilustrowano rozwiązania dla różnych liczb falowych i różnych rozpraszaczy. Przydatność takiej metody symulacji została przedyskutowana z punktu widzenia tomografii akustycznej. (Modelowanie numeryczne problemów rozpraszania akustycznego i ultradźwiękowego z arbitralnie ukształtowanym rozpraszaczem).

**Keywords:** ultrasound tomography, scattering problems, rekonstrukcja obrazu  
**Słowa kluczowe:** tomografia ultradźwiękowa, problemy z rozpraszaniem, image reconstruction

## Introduction

BEM is the preferable approach to acoustic scattering problems in infinite domains. The biggest advantage is that the Sommerfeld radiation condition [1] is automatically satisfied by BEM open boundary problem. Thus, there is no requirement to truncate the domain and impose artificial non-reflecting boundary conditions. By High-Frequency 2D Scattering Problems, we understand the problems in which the Reynolds Scattering criteria [2] are not fulfilled. It means that the wavelength is much smaller than the dimensions of the scatterer.

The exterior acoustic problem is described by the Helmholtz equation of the form [3,4,5]:

$$(1) \quad \nabla^2 \varphi(\mathbf{p}) + k^2 \varphi(\mathbf{p}) = Q,$$

where  $\varphi(\mathbf{p})$  [m<sup>2</sup>/s], is the scalar velocity potential amplitude,  $k^2 = \frac{\omega^2}{c^2}$  is the wavenumber [1/m<sup>2</sup>],  $\omega = 2\pi f$  [1/s],  $c$  [m/s] is the propagation velocity and the wavelength is equal to  $\lambda = c/f$  [m].

The right-hand side  $Q$  [1/s] stands for the acoustic source. The complex-valued function  $\varphi(\mathbf{p})$  possess the magnitude and phase shift [6].

In theoretical acoustics [6], it is often desirable to work with the Helmholtz equation (1) of the velocity potential  $\varphi$  instead of pressure  $p$  and/or vector of the particle velocity  $\mathbf{v}$ . Taking into account the above considerations and making use of Green's second identity, the Helmholtz equation (1) can be expressed in an equivalent form of a Boundary Integral Equation (BIE) [1], i.e.

$$(2) \quad \int_{\Gamma} \frac{\partial G(|\mathbf{r}-\mathbf{r}'|)}{\partial n} \varphi(\mathbf{r}') d\Gamma = \int_{\Gamma} G(|\mathbf{r}-\mathbf{r}'|) \frac{\partial \varphi(\mathbf{r}')}{\partial n} d\Gamma + \varphi^{inc}(\mathbf{r}), \quad \mathbf{r} \in \Gamma$$

where  $\varphi^{inc}$  is the incident wave, and the vector  $\mathbf{n}$  is the unit normal vector outward pointing from the considered domain (see Fig. 1).

The sound-hard scatterer is imposed through a homogeneous Neumann boundary condition on the boundary  $\Gamma = I \cup S$  (see Fig. 2). Due to the homogeneous Neumann boundary conditions, the third term of equation (2) vanish. Now, the boundary integral equation (2) for constant boundary elements can be written in terms of local coordinate  $\xi$  as follows:

$$(3) \quad c(\mathbf{r})\varphi(\mathbf{r}) + \sum_{j=1}^M \varphi_j(\mathbf{r}') \int_{-1}^{+1} \frac{\partial G(|\mathbf{r}-\mathbf{r}'|)}{\partial n} J(\xi) d\xi = \varphi^{inc}(\mathbf{r})$$

where  $M$  – is the total number of constant elements, and  $J(\xi)$  – is the Jacobian of transformation defined as:

$$J(\xi) = \frac{d\Gamma}{d\xi} = \sqrt{\left(\frac{dx(\xi)}{d\xi}\right)^2 + \left(\frac{dy(\xi)}{d\xi}\right)^2} = \frac{L}{2},$$

where  $L$  is the length of the constant boundary element [7-10].

If the plane wave is travelling along the vector  $\mathbf{d}_j = (\cos \theta_j, \sin \theta_j)$  than  $\varphi^{inc}(\mathbf{r}) = e^{i\mathbf{k}\mathbf{r}\cdot\mathbf{d}_j}$ , where  $i = \sqrt{-1}$  is the imaginary unit.

Using the above relations, the incoming wave is relatively easy to calculate on the boundary and incorporate it into the right-hand side of the equation (3).

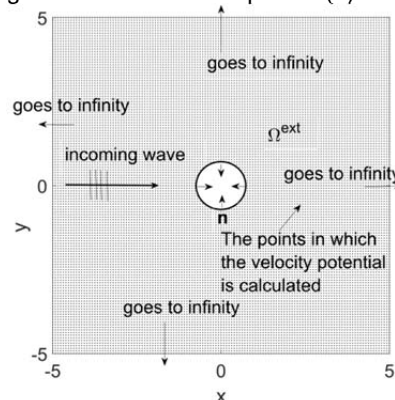


Fig. 1. External region under consideration illuminated by plane time harmonic incoming wave  $c(\mathbf{r})\varphi(\mathbf{r}) +$

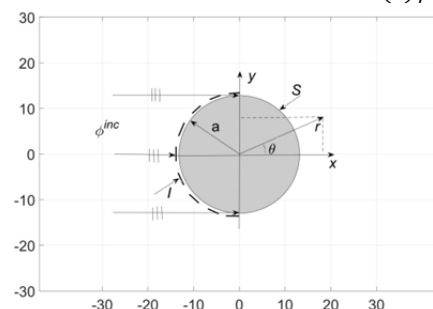


Fig. 2. Circular scatterer illuminated by plane wave where I denote the illuminated and S denotes the shadow zone

### Plane wave and arbitrarily shaped scatterer benchmark

Many methods can be used to solve direct, inverse and optimization problems [11-21]. Let us consider the scattering problem for a high-frequency regime, i.e., when the wavelength of the incoming wave is much less than the diameter of the scatterer. In the experiment, we have considered examples starting from the wavelength 0.63 m up to 0.013 m when the dimensions of the scatterers were about 2 m. So, we can say that high-frequency regime conditions were fulfilled.

The simulation of the scattering problems is an extremely difficult task. The BEM results could be reliable if the following criteria were considered. Moreover, here are the most important of them:

- 1) The number of boundary elements should be no less than 6 to 10 for the wavelength (see, for example [22]),
- 2) it is well known in the literature that BEM provide unreliable results for all but low wavenumber [9]. Additionally, the wavenumber should fulfil the following relation:

$$(4) \quad kD < 4.0$$

where  $D$  denote the diameter of the body, and when the shape of the body is irregular, then the maximum distance between two boundary points. In [9], the author states this is too restrictive for most applications. In our simulation, not all cases fulfilled this condition, but the results were satisfactory despite that.

### Convex scatterer

In this section, we will deal with a square-shaped scatterer. This is a more challenging problem than the smooth convex obstacle like the circle since the corners of the polygon give rise to strong diffracted rays, which illuminate the shadow side of the obstacle much more strongly than the rays that creep into the shadow zone of a smooth convex obstacle [5].

The shadow or the illuminated zones (the zone consists of collection of boundary elements) could be calculated in the following way:

$$(5) \quad \mathbf{n}_j \cdot \mathbf{d} > 0$$

where the plane wave is travelling along the unite vector  $\mathbf{d} = (\cos \theta, \sin \theta)$  and  $\mathbf{n}_j$  is the united normal vector of boundary element, directed outside the investigated region (see Fig. 1). So, the dot product  $\mathbf{n}_j \cdot \mathbf{d}$  after some mathematics is equal  $n_{jx} \cos \theta + n_{jy} \sin \theta = \cos \theta_j \cos \theta + \sin \theta_j \sin \theta$  (see Fig. 2). The angle of  $\theta_j$  is the angle of the position vector of particular boundary element [5].

In all numerical experiments, the scatterer boundaries were rigid (modelled by the homogeneous Neumann boundary conditions) and were discretised by constant boundary elements. The number of boundary elements was selected so that the wavelength  $\lambda$  per element length was as high as possible. For considered cases, the ratio is shown in table 1.

The figures below show the situation when the incoming wave has a direction vector with an angle equal to zero, counting in a counterclockwise direction from the positive x-axis. It means that the flat wave is coming from the square scatterer's left side to the scatterer's right side (see Fig. 4).

In the presence of corners (see Fig. 3), the classical BEM is not capable of achieving engineering accuracy (for which according to [6] is taken a common definition of 1% error) due to highly oscillating velocity potential (consult Fig. 3c) even for relatively low (acoustical) frequencies. Some authors apply an enriched basis function. However, it is not the topic of this paper. Interested readers should find more

details in [9]. As we can see in Fig. 4, when the frequency becomes higher, for the classical BEM more and more boundary elements are necessary to maintain the reasonable ratio of the boundary elements per wavelength. For the last two frequencies, 6022 and 9800 Hz, the boundary elements per wavelength are 7 and 5, respectively, below the recommended value.

Now we consider an incident plane wave propagating in an angle of  $-\pi/4$ , which means that the flat incoming wave propagates from the upper left corner to the lower right corner.

When the angle of the incoming wave is different from zero, the field pattern around the square scatterer becomes more interesting. For all cases, the basic acoustical data are assembled in table 1.

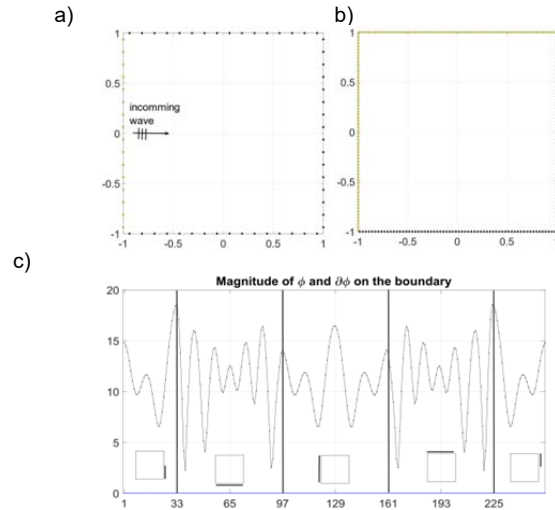
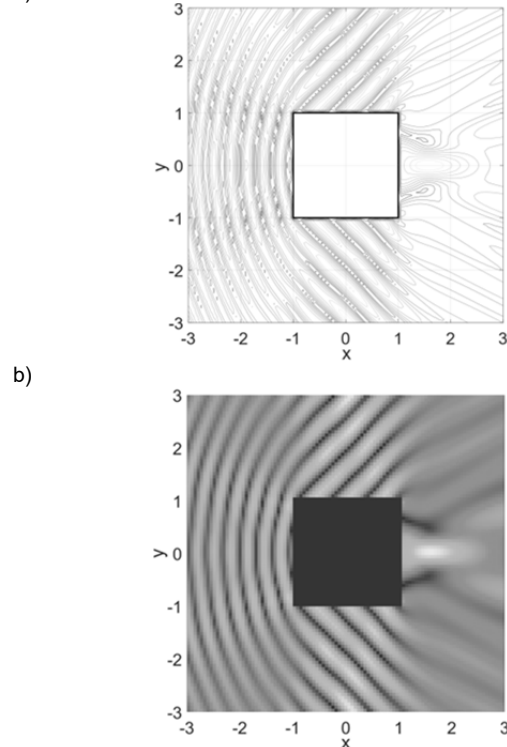


Fig. 3. Single square scattering object a) incoming flat wave from left to right and illumination (yellow) and shadowed side (black) of the boundary b) incoming wave from left upper corner to lower right corner of square scatterer and illuminated and shadowed boundaries marked by yellow and black colour respectively c) magnitude velocity potential distribution on the perimetry of the boundary as it is indicated in the bottom of the figure



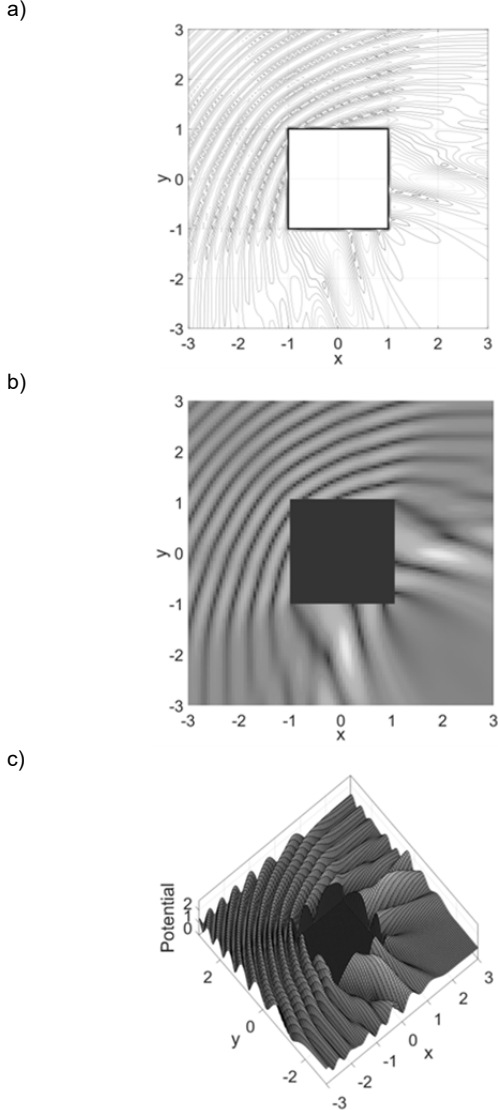
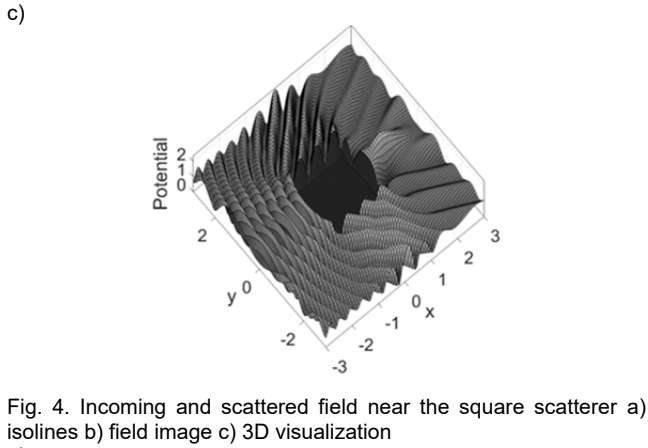


Fig. 5. Incoming and scattered field near the square scatterer a) isolines b) field image c) 3D visualization

Table 1. Basic acoustical data for numerical experiment with square scatterer

Acoustical data for the figures	wavelength $\lambda$ [m]	$\lambda / L$	wave number $k$ [1/m]	Frequency $f$ [Hz]
4 and 5	0.630	20	10	547.50
	0.160	10	40	2190.
	0.057	7	110	6022.
	0.035	5	179	9800.

It is not possible to increase the frequency up to the ultrasonic level without dramatic incrementation of discretization density. So, the geometrical dimensions were rescaled to keep the above-mentioned criteria of proper numerical simulation. It means that the dimensions of the scatterer were adjusted to the ultrasound wavelength.

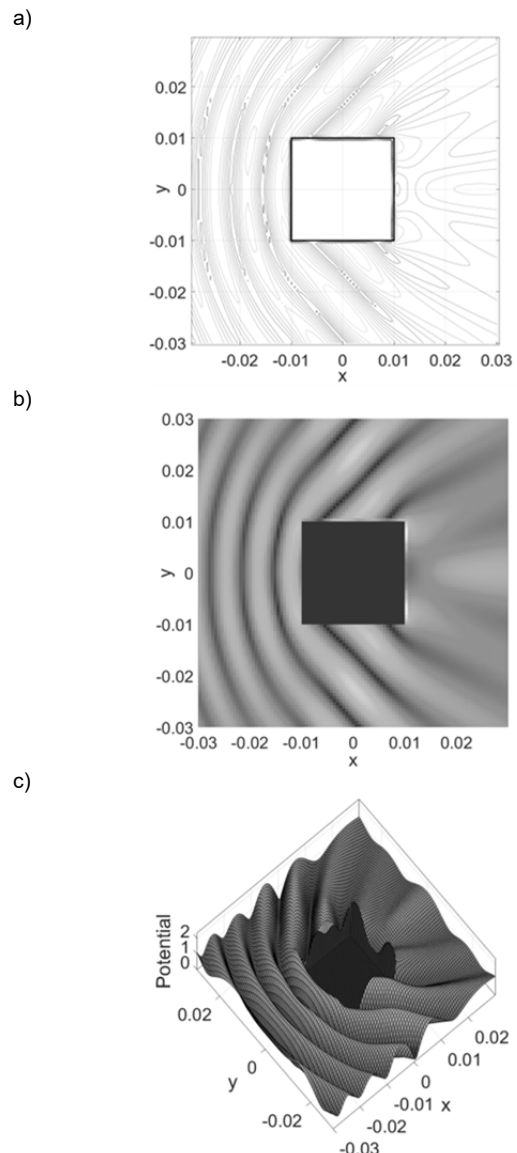


Fig. 6. Incoming and scattered high frequency (USG) field near the square scatterer a) isolines b) field image c) 3D visualization

After resizing, the geometrical dimensions of the scatterer are small enough to fulfil the demands of the number of boundary elements per wavelength equal to at least 10. This case equals  $\lambda/n = 0.013/0.0078125 \cong 160$  for the frequency  $f = 27375$  Hz. So, it is much more than our demand.

As a next example, let's consider the corrugated circle-shaped scatterer. With significantly deep corrugations of the scatterer's boundary, it can easily see shadowed and illuminated parts of the boundary (see Fig. 7).

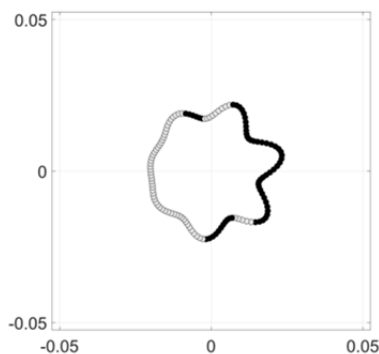
## Conclusions

This paper presented an acoustic scattering problem in 2D space for high frequency and for an arbitrary shape of the scatterers. The classical BEM was used for acoustic and ultrasound problems, but always keeping in mind the criteria mentioned above of the correct solution.

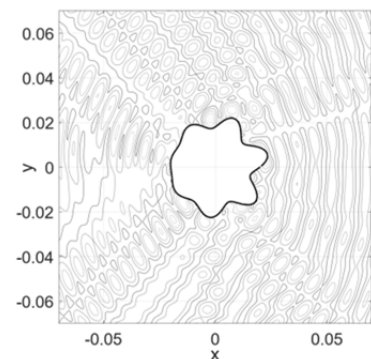
On this basis, we can state that the literature demand concerns the lower limit of the number of boundary elements per wavelength might be insufficient in case of the inverse problem, particularly for the ultrasonic frequency wave bound.

The main goal of this paper was to investigate if the classical boundary element method might be suitable for tomography problems in acoustic and ultrasonic problems. However, more sophisticated basis functions might be necessary for more complicated shapes of scatterers, as shown in the square scatterer's case for the high frequency. The number of elements per wavelength became so high that it could be impossible to use a presented version of BEM for tomography problems.

a)



b)



c)

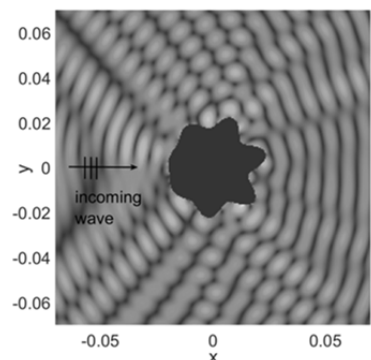


Fig. 7. Corrugated circle-shaped scatterer a) illuminated and shadowed zones b) isolines of the acoustic field c) image of the field and direction of the incoming flat wave

**Authors:** prof. dr hab. inż. Jan Sikora<sup>1,2</sup>, e-mail: sik59@wp.pl, Research & Development Centre Netrix S.A., Związkowa 26, 20-148 Lublin, Poland; University of Economics and Innovation in Lublin, ul. Projektowa 4, 20-209 Lublin, Poland;

#### REFERENCES

[1] Colton, D., Kress, R., Integral Equation Methods in Scattering Theory, Springer, (1993).

- [2] Baynes A.B., Scattering of low-frequency sound by compact objects in underwater waveguides, Naval Postgraduate School, Monterey, California, PhD Dissertation, (2018).
- [3] Becker A.A., The boundary Element Method in Engineering. A complete course. McGraw-Hill Book Company, (1992).
- [4] Cakoni F., Colton D., A Qualitative Approach to Inverse Scattering Theory, Applied Mathematical Sciences, 188 (2014), ISBN 978-1-4614-8827-9 (eBook)
- [5] Chandler-Wilde S.N., Langdon S., A Galerkin Boundary Element Method for high frequency scattering by convex polygons, SIAM J. NUMER. ANAL., 45 (2007), No. 2, 610–640
- [6] Gilvey B., J. Trevelyan J., Hattori G., Singular enrichment functions for Helmholtz scattering at corner locations using the Boundary Element Method, Int. J. Numer. Meth. Engng, (2017); 00:1–16, DOI: 10.1002/nme
- [7] Akylas T.R., Mei C.C., I-campus project School-wide Program on Fluid Mechanics Modules on Waves in fluids. Chapter Five of Reflection, Transmission and Diffraction. <http://web.mit.edu/fluids-modules/waves/www/c-index.html>
- [8] Rymarczyk T., Tomographic Imaging in Environmental, Industrial and Medical Applications, Innovatio Press Publishing Hause, (2019).
- [9] Jabłoński P., Engineering Physics – Electromagnetism, Częstochowa University of Technology, (2009).
- [10] Kirkup S., The Boundary Element Method in Acoustics, Book in Journal of Computational Acoustics, January (2007).
- [11] Kania, W., Wajman, R., Ckript: a new scripting language for web applications, Informatyka, Automatyka, Pomiary W Gospodarce I Ochronie Środowiska, 12(2022), No. 2, 4-9.
- [12] Styła, M., Adamkiewicz, P., Hybrid navigation system for indoor use. Informatyka, Automatyka, Pomiary W Gospodarce I Ochronie Środowiska, 12 (2022), No. 1, 10-14.
- [13] Sikora R., Markiewicz P., Korzeniewska E., Using identification method to modelling short term luminous flux depreciation of LED luminaire to reducing electricity consumption, Scientific Reportst, 13 (2023), No. 1, 673.
- [14] Lebioda, M., Korzeniewska, E., The Influence of Buffer Layer Type on the Electrical Properties of Metallic Layers Deposited on Composite Textile Substrates in the PVD Process, Materials, 16 (2023), No. 13, 4856.
- [15] Rymarczyk T., Kozłowski E., Kłosowski G., Electrical impedance tomography in 3D flood embankments testing – elastic net approach, Transactions of the Institute of Measurement and Control, 42 (2020), No. 4, 680-690.
- [16] Kłosowski G., Rymarczyk T., Niderla K., Rzemieniak M., Dmowski A., Maj M., Comparison of Machine Learning Methods for Image Reconstruction Using the LSTM Classifier in Industrial Electrical Tomography, Energies 2021, 14 (2021), No. 21, 7269.
- [17] Rymarczyk T., Kłosowski G., Hoła A., Sikora J., Tchórzewski P., Skowron Ł., Optimising the Use of Machine Learning Algorithms in Electrical Tomography of Building Walls: Pixel Oriented Ensemble Approach, Measurement, 188 (2022), 110581.
- [18] Koulountzios P., Rymarczyk T., Soleimani M., A triple-modality ultrasound computed tomography based on full-waveform data for industrial processes, IEEE Sensors Journal, 21 (2021), No. 18, 20896-20909.
- [19] Koulountzios P., Aghajanian S., Rymarczyk T., Koironen T., Soleimani M., An Ultrasound Tomography Method for Monitoring CO2 Capture Process Involving Stirring and CaCO3 Precipitation, Sensors, 21 (2021), No. 21, 6995.
- [20] Kłosowski G., Rymarczyk T., Niderla K., Kulisz M., Skowron Ł., Soleimani M., Using an LSTM network to monitor industrial reactors using electrical capacitance and impedance tomography – a hybrid approach. Eksploatacja i Niezawodność – Maintenance and Reliability, 25 (2023), No. 1, 11.
- [21] Kłosowski G., Rymarczyk T., Kania K., Świć A., Cieplak T., Maintenance of industrial reactors supported by deep learning driven ultrasound tomography, Eksploatacja i Niezawodność – Maintenance and Reliability; 22 (2020), No 1, 138–147.
- [22] Kirkup S., The Boundary Element Method in Acoustics: A Survey, Article in Applied Sciences, April (2019), DOI: 10.3390/app9081642